Structural Performance and Failure Probability Analysis of Steel Truss Bridges

Jia Gao

School of Economics and Management, Tianjin University of Science and Technology, Tianjin, China

wxn20040315@mail.tust.edu.cn

Abstract. Study presents a comprehensive analysis of the structural performance and failure probability of a steel truss pedestrian bridge. The load transfer mechanism was analyzed under dead and live loads, including bridge self-weight (15 kN/m), deck weight (15 kN/m), crowd load (27 kN/m), and vehicle load (11 kN/m). Stability analysis was conducted using joint and section methods, validated through finite element software. A probabilistic framework employing Monte Carlo simulation (1,000 samples) evaluated failure risks, considering lognormal-distributed nodal forces (mean=5.378 kN, COV=0.3) and rod diameters (mean=0.1 m, COV=0.02). The results obtained from this analysis revealed a system-level failure probability of 15%, which was attributed to series-structure dependency. This analysis also highlighted the sensitivity of the system to material variability and sample size. The implementation of mitigation strategies, encompassing material substitution (Q235 steel) and variance reduction techniques, led to a substantial reduction in failure probability to 2%. This research underscores the necessity of probabilistic methods in enhancing urban bridge safety and reliability, aligning with advancements in structural engineering and risk management.

Keywords: Truss Carlo, probability analysis.

1. Introduction

Steel truss bridges have been defined by their design flexibility and structural performance, enabling economical construction in an urban environment [1]. Triangular truss structures' simplicity of shape means material to use with a load-carrying capacity, thereby achieving urban planning goals of sustainability [2]. Beyond their application purpose, such bridges have also been significant design icons, with beauty and structural integrity achieved to perfection [3].

Classical deterministic theories fail to accommodate built-in variabilities in material properties and loads, which could result in underestimating failure hazards [2]. Contemporary literature, e.g., Liu et al. [3], articulates the imperative need for probabilistic methods in modelling yield strength distribution. At the same time, Xie and Li [4, 5] confirmed the prospective function of random damage growth in composite structures. For steel truss bridges, probabilistic methods enable cohesive evaluation of security margins based on nodal force uncertainty, cross-sectional sizes, and load combinations. The bridge enables quick installation in areas with scant spaces, for example, footbridges over highways or rivers [6]. So it is especially pertinent to urban infrastructure, for failure affects economic loss and societal disruption. While academic studies have considered the structural performance of steel truss bridges, the general application of probabilistic failure analysis remains rare. This study attempts to close this gap by adding a Monte Carlo-based probabilistic approach to failure estimation under real-world conditions. This research intends to:

1) The goal is to develop a simplified two-dimensional analytical model to identify a steel truss bridge's load transfer and stability.

2) The quantification of failure probabilities is to be achieved using Monte Carlo simulation, incorporating material and load uncertainties.

3) The study will propose design to enhance the structural reliability, which will be validated through comparative case studies.

Probabilistic frameworks serve to address the discrepancy between models and real-world performance. By addressing variability in critical parameters (e.g. rod diameters and nodal forces), engineers design resilient structures capable of withstanding unforeseen stressors [7]. In the context of urban steel truss bridges, the implementation of such methodologies has been shown to result in a reduction in lifecycle costs and an extension in service life, thereby guaranteeing prolonged-term safety and sustainability [8].

2. Method

2.1. Struktural Parameters

To this structure, it is important to know how the load is transmitted. From Figure 1, suppose there is a man on the bridge, this will give a force to the deck, and the force will be transmitted to the longitudinal beam, and then to the joint, and to the rod, and finally to this analysis can know that this is a complex 3D problem which is not easy to , but find that the load is transferred from the bridge deck to both sides of the truss bears the load only on its plane, so we can reduce it to a 2D problem, it becomes very easy to figure simplified it to a 2D problem, let's look at the structure and dimensions of the truss bridge. It has 3 types of bars, top bar, bottom bar and diagonal bar. This bridge is an model, each length is 4 and each angle is Figure3.So we can conclude that:

Geometric Configuration: A symmetrical truss bridge with a span of 4 meters, comprising top, bottom, and diagonal rods at 60° angles (Figure 1).

Material Properties: Steel (Young's modulus: 210 GPa, yield strength: 235 MPa), circular cross-sections (diameter: 0.1 m).

Load Transfer Mechanism: Distributed forces from the deck transfer to longitudinal beams, joints, and supports, simplified to 2D plane analysis.

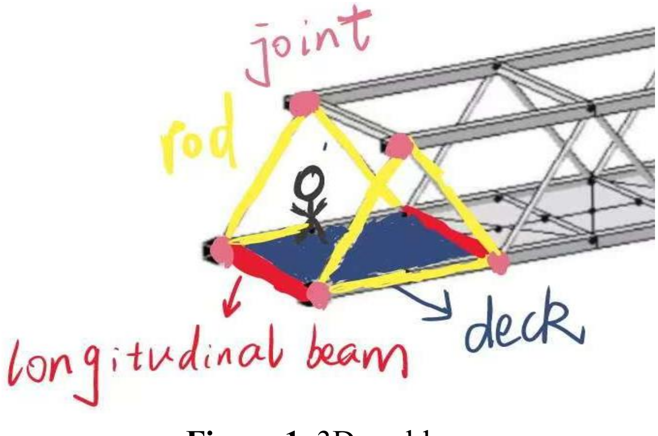

Figure 1. 3D problem

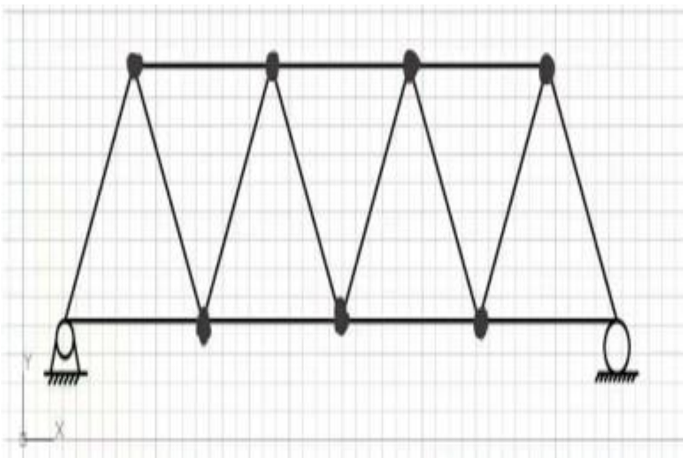

Figure 2. 2D problem

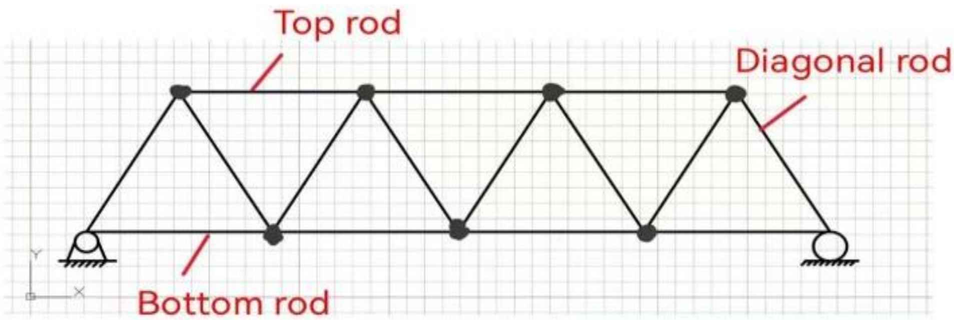

Figure 3. Composition of structure

2.2. Loads Analysis

Two load types will be considered: dead load and live dead load comprises the bridge body weight (15 kilonewtons per) and deck weight (15 kilonewtons per). The live load, on the other hand, is comprised of the weight of the crowd and cars. The former is 27 kilonewtons per, and the latter is 11 kilonewtons per. It is important to note that all these forces are considered these data points, the analysis of the bridge structure can commence. To illustrate this, we will examine the live load depicted in Figure 4. In Figure 4, joint A exhibits bilateral distribution of forces, with the force range on one side of the rod measuring 2. The total distance is therefore 4. The force exerted on joint A is calculated by multiplying 38 kN/m by 4, yielding a resultant force of 15.6 kN. The same calculation method can be applied to joints B and C. For joints E and D, only the left or right side of the distributed force is present. However, it is known to be collinear with the reaction force of support. Therefore, it is regarded as a new force, and no additional force is required in this can therefore be concluded that:

Table 1. Loads data

Numble	Dead loads		Live loads		Mathematical Modeling
1	Self-weight	Deck weight	Crowd load	Vehicle load	Joint A
2	15kN/m (uniformly distributed).	15kN/m (transferred to longitudinal beams).	27kN/m (dynamic, modeled as static equivalent) [6].	11kN/m (simplified to point loads at joint).	Total load =38kN/m×4m=152kN. Equilibrium equations resolved via matrix methods).

2.3. Stabilste Analysis

To analyze the structure, the load conditions and dimensions must first be considered. In this case, three key questions must be addressed: first, the reaction forces need to be calculated; second, the internal forces within each rod must be determined; and finally, the structural stability must be assessed. It is important to note that the structure is symmetrical, allowing the analysis to focus on only one half. The joint method and the section method are the primary analytical tools employed in this study, supplemented by the force equilibrium equations. The calculations yielded the internal forces of each rod, as shown in Figure 4. It was observed that some bars were subjected to tension, while others experienced compression. To accommodate this, materials with high compressive strength were selected for the red bars, and those with high tensile strength for the blue bars. The structural integrity of the model was then verified using simulation software, which produced consistent results (see Figure 5). Based on the analysis, the following data was obtained:

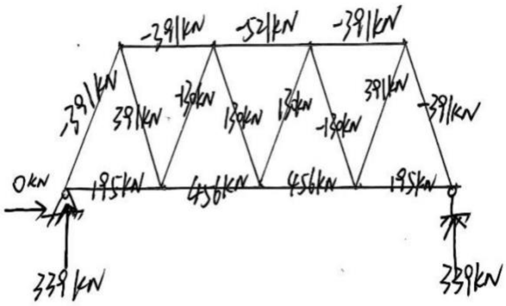

Figure 4. The force of each rod

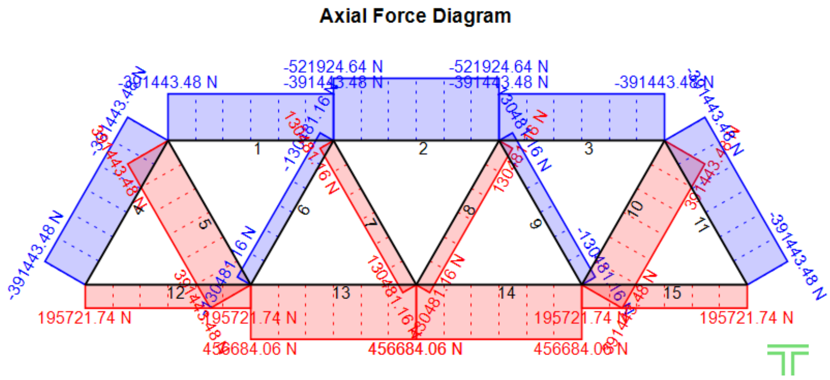

Figure 5. Software analyse

Table 2. Forces data

Numble	Reaction Forces:	Member Forces:		Validation:
1	Symmetry exploited to calculate vertical reactions (RA=RB=190 kN).	Tension members (blue): Maximum force = 215 kN (diagonal rods).	Compression members (red): Maximum force = 198 kN (top rods).	Finite element analysis (Figure 5) confirmed force distributions with <5% error [10].

2.4. Faulere Probabilist Analyze

The variable X represents the nodal force, which follows a lognormal distribution with a mean of 5.3782 kN and a coefficient of variation of 0.3. Based on these values, the standard deviation of the nodal force is calculated. The variable Y represents the diameter of the rod, which also follows a lognormal distribution with a mean of -2.308 and a standard deviation of 0.02. To simplify subsequent analysis, the diameter is used to estimate the rod's cross-sectional area, S, by calculating the area using the formula for a circle. The cumulative distribution function (CDF) for the area S is then determined. The Monte Carlo simulation is performed using Excel to conduct the analysis. The Monte Carlo simulation is performed using Excel.

Random variable selection table

Name	Relevant distribution	Standard deviation Mean value	Reason
X--Node stress	lognormal distribution	$\mu = \ln(226) - \frac{\sigma^2}{2} = 5.3782$ $\sigma = \ln\sqrt{1+COV^2} = 0.2936$	The COV is set at 15% to 30%.In order to achieve a greater degree of dispersion and in accordance with the reference[1], it is set at 30%.
Y--The diameter of the rod	lognormal distribution	$\mu = \ln(0.1) - \frac{\sigma^2}{2} = -2.3028$ $\sigma = \ln\sqrt{1+COV^2} = 0.02$	The diameter error is caused by processing and is a minor one. We take 2% as the tolerance. (GB/T 1804-2000)

Figure 6. Random variable selection table

Initially, the force on the node is simulated, followed by the generation of one thousand sets of data to obtain its CDF. The random function in Excel is employed to randomly generate numbers within the range of 0 to 1. The inverse CDF is derived using the Excel function LOGNORM.INV (probability, mean, standard). Reverse the process to obtain the CDF, and then calculate the sample (Figure 7).

1		LOGNARM.DIST Function		
2				
3		Description		Date
4		Mean of int (x)		5.3782
5		Standard deviation of int (x)		0.2936
6				
7				
8	Trail	Rand	Inverse CDF	
9	1	0.2054465	170.16455	
10	2	0.1095915	151.02609	
11	3	0.2001726	169.23376	
12	4	0.2988671	185.5415	
13	5	0.1680283	163.32808	
14	6	0.4942096	215.71076	
15	7	0.6763407	247.77453	
16	8	0.8681171	300.75865	
17	9	0.7559833	265.54757	
18	10	0.6113619	235.39166	
19	11	0.6168358	236.38275	
20	12	0.5784416	229.59247	
21	13	0.3648302	195.73046	
22	14	0.7630051	267.3125	
23	15	0.7504544	264.18516	
24	16	0.446188	208.19526	
25	17	0.4050751	201.87885	
26	18	0.5419888	223.44355	
27	19	0.9957695	469.31673	
28	20	0.2684545	180.71185	
29	21	0.7776473	271.12776	
30	22	0.0793639	143.22415	
31	23	0.1361487	156.94409	
32	24	0.5868503	231.04917	
33	25	0.9849119	409.38555	

Sheet1 Sheet2 Sheet3 Sheet4 Sheet5 +

Figure 7. Monte Carlo simulation process for X variables nodal force

The next step in the process is to simulate the diameter of the rod to obtain its cumulative distribution function (CDF). The CDF of area S is then obtained by employing the CDF of diameter through area formula (Figure 8).

1		LOGNARM.DIST Function		
2				
3		Description		Date
4		Mean of int (y)		-2.3028
5		Standard deviation of int (y)		0.02
6				
7				
8	Trail	Rand	Inverse CDF	
9	1	0.577424	0.0079122	
10	2	0.7739543	0.0080903	
11	3	0.5579496	0.0078965	
12	4	0.5217816	0.0078678	
13	5	0.7412006	0.0080564	
14	6	0.4998495	0.0078505	
15	7	0.6118826	0.0079404	
16	8	0.8424821	0.0081725	
17	9	0.5613625	0.0078992	
18	10	0.7191446	0.008035	
19	11	0.8736767	0.0082182	
20	12	0.1916122	0.0075815	
21	13	0.7999216	0.0081193	
22	14	0.0852148	0.0074317	
23	15	0.2609757	0.0076521	
24	16	0.8907469	0.0082467	
25	17	0.6729278	0.0079926	
26	18	0.0309092	0.0072855	
27	19	0.4747189	0.0078307	
28	20	0.7493169	0.0080646	
29	21	0.1213004	0.0074921	
30	22	0.0532535	0.0073598	
31	23	0.0976039	0.0074542	
32	24	0.5242356	0.0078697	
33	25	0.9964026	0.0087416	

Sheet1 Sheet2 Sheet3 Sheet4 Sheet5 +

Figure 8. Monte Carlo simulation of the cross-sectional area of a rod

After that, the forces on the other eight rods are obtained through force analysis, their algebraic relationship is obtained by force analysis diagrams (Figure 9), and their CDF are calculated through algebraic relationships using the CDF of the nodal forces (Figure 10).

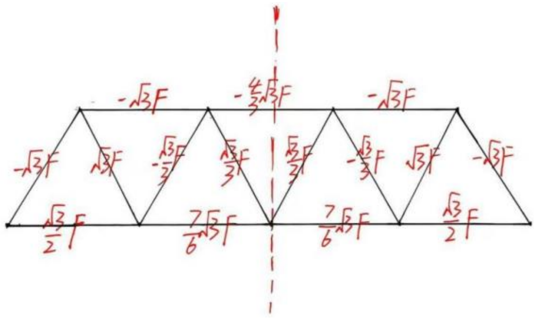

Figure 9. Force analysis diagram

		F1 CDF	F2 CDF	F3 CDF	F4 CDF	F5 CDF	F6 CDF	F7 CDF	F8 CDF
2	1	-294.734	-392.978	-294.734	294.7336	-98.2445	98.24455	147.3668	343.8559
3	2	-261.585	-348.78	-261.585	261.5849	-87.195	87.19495	130.7924	305.1823
4	3	-293.121	-390.829	-293.121	293.1215	-97.7072	97.70716	146.5607	341.9751
5	4	-321.367	-428.49	-321.367	321.3673	-107.122	107.1224	160.6837	374.9285
6	5	-282.893	-377.19	-282.893	282.8925	-94.2975	94.29751	141.4463	330.0413
7	6	-373.622	-498.163	-373.622	373.622	-124.541	124.5407	186.811	435.8923
8	7	-429.158	-572.211	-429.158	429.1581	-143.053	143.0527	214.579	500.6844
9	8	-520.929	-694.572	-520.929	520.9293	-173.643	173.6431	260.4646	607.7508
10	9	-459.942	-613.256	-459.942	459.9419	-153.314	153.314	229.9709	536.5989
11	10	-407.71	-543.614	-407.71	407.7103	-135.903	135.9034	203.8552	475.662
12	11	-409.427	-545.903	-409.427	409.4269	-136.476	136.4756	204.7135	477.6647
13	12	-397.666	-530.221	-397.666	397.6658	-132.555	132.5553	198.8329	463.9435
14	13	-339.015	-452.02	-339.015	339.0151	-113.005	113.005	169.5076	395.5176
15	14	-462.999	-617.332	-462.999	462.9988	-154.333	154.3329	23[illegible]4994	540.1653
16	15	-457.582	-610.109	-457.582	457.5821	-152.527	152.5274	228.7911	533.8458
17	16	-360.605	-480.806	-360.605	360.6048	-120.202	120.2016	180.3024	420.7056
18	17	-349.664	-466.219	-349.664	349.6644	-116.555	116.5548	174.8322	407.9418
19	18	-387.016	-516.021	-387.016	387.0156	-129.005	129.0052	193.5078	451.5182
20	19	-812.88	-1083.84	-812.88	812.8804	-270.96	270.9601	406.4402	948.3605
21	20	-313.002	-417.336	-313.002	313.0021	-104.334	104.334	156.5011	365.1691
22	21	-469.607	-626.143	-469.607	469.6071	-156.536	156.5357	234.8035	547.8749
23	22	-248.072	-330.762	-248.072	248.0715	-82.6905	82.6905	124.0358	289.4168
24	23	-271.835	-362.447	-271.835	271.8351	-90.6117	90.61171	135.9176	317.141
25	24	-400.189	-533.585	-400.189	400.1889	-133.396	133.3963	200.0945	466.8871
26	25	-709.077	-945.435	-709.077	709.0766	-236.359	236.3589	354.5383	827.256
27	26	-406.239	-541.653	-406.239	406.2395	-135.413	135.4132	203.1197	473.9461
28	27	-242.049	-322.732	-242.049	242.0492	-80.6831	80.68305	121.0246	282.3907
29	28	-243.941	-325.254	-243.941	243.9405	-81.3135	81.31351	121.9703	284.5973
30	29	-426.967	-569.289	-426.967	426.9667	-142.322	142.3222	213.4833	498.1278
31	30	-380.287	-507.049	-380.287	380.287	-126.762	126.7623	190.1435	443.6682
32	31	-607.257	-809.677	-607.257	607.2574	-202.419	202.4191	303.6287	708.467
33	32	-384.383	-512.51	-384.383	384.3825	-128.128	128.1275	192.1913	448.4463
34	33	-347.195	-462.927	-347.195	347.1953	-115.732	115.7318	173.5977	405.0612
35	34	-480.405	-640.54	-480.405	480.4048	-160.135	160.1349	240.2024	560.4722
36	35	-476.808	-635.744	-476.808	476.8079	-158.936	158.936	238.4039	556.2759
37	36	-399.196	-532.261	-399.196	399.1956	-133.065	133.0652	199.5978	465.7282
38	37	-213.661	-284.881	-213.661	213.6608	-71.2203	71.22028	106.8304	249.271
39	38	-395.668	-527.558	-395.668	395.6682	-131.889	131.8894	197.8341	461.6129

Sheet1 Sheet2 Sheet3 Sheet4 Sheet5

Figure 10. CDF of 8 rods

Finally, the stresses were calculated for each bar compared to the yield stress of 100 MPA, using Excel to filter out data >100 MPA, which means that this bar will fail (Figure11 and Figure12).

F1/S	F2/S	F3/S	F4/S	F5/S	F6/S	F7/S	F8/S
56840.3616	75787.1488	56840.3616	56840.3616	18946.7872	18946.78719	28420.1808	66313.75517
56504.9225	75339.8967	56504.9225	56504.9225	18834.9742	18834.97418	28252.4613	65922.40964
56724.4733	75632.631	56724.4733	56724.4733	18908.1578	18908.15776	28362.2366	66178.55216
44338.6619	59118.2159	44338.6619	44338.6619	14779.554	14779.55398	22169.331	51728.43892
51921.7587	69229.0115	51921.7587	51921.7587	17307.2529	17307.25289	25960.8793	60575.38511
33193.1306	44257.5074	33193.1306	33193.1306	11064.3769	11064.37686	16596.5653	38725.31901
74180.8412	98907.7882	74180.8412	74180.8412	24726.9471	24726.94706	37090.4206	86544.3147
71988.1427	95984.1903	71988.1427	71988.1427	23996.0476	23996.04758	35994.0714	83986.16653
44039.3271	58719.1027	44039.3271	44039.3271	14679.7757	14679.77569	22019.6635	51379.2149
39018.0503	52024.067	39018.0503	39018.0503	13006.0168	13006.01676	19509.0251	45521.05866
36147.4517	48196.6023	36147.4517	36147.4517	12049.1506	12049.15058	18073.7259	42172.02703
32840.2112	43786.9483	32840.2112	32840.2112	10946.7371	10946.73707	16420.1056	38313.57974
58607.648	78143.5307	58607.648	58607.648	19535.8827	19535.88267	29303.824	68375.58936
75808.8624	101078.483	75808.8624	75808.8624	25269.6208	25269.6208	37904.4312	88443.67281
76792.7913	102390.388	76792.7913	76792.7913	25597.5971	25597.59709	38396.3956	89591.58981
46924.0456	62565.3941	46924.0456	46924.0456	15641.3485	15641.34852	23462.0228	54744.71983
49548.8643	66065.1525	49548.8643	49548.8643	16516.2881	16516.28811	24774.4322	57807.0084
42854.9108	57139.8811	42854.9108	42854.9108	14284.9703	14284.97027	21427.4554	49997.39594
87956.6304	117275.507	87956.6304	87956.6304	29318.8768	29318.87679	43978.3152	102616.0688
56850.6408	75800.8544	56850.6408	56850.6408	18950.2136	18950.21359	28425.3204	66325.74756
77993.499	103991.332	77993.499	77993.499	25997.833	25997.833	38996.7495	90992.41551
44515.8753	59354.5003	44515.8753	44515.8753	14838.6251	14838.62509	22257.9376	51935.1878
52303.1186	69737.4915	52303.1186	52303.1186	17434.3729	17434.37287	26151.5593	61020.30506
29785.3837	39713.8449	29785.3837	29785.3837	9928.46123	9928.461228	14892.6918	34749.6143
32243.9424	42991.9231	32243.9424	32243.9424	10747.9808	10747.98079	16121.9712	37617.93276
62756.724	83675.6321	62756.724	62756.724	20918.908	20918.90801	31378.362	73216.17805
60657.83	80877.1067	60657.83	60657.83	20219.2767	20219.27667	30328.915	70767.46836
64885.8304	86514.4405	64885.8304	64885.8304	21628.6101	21628.61013	32442.9152	75700.13546
60670.4529	80893.9371	60670.4529	60670.4529	20223.4843	20223.48429	30335.2264	70782.195
45906.8563	61209.1418	45906.8563	45906.8563	15302.2854	15302.28544	22953.4282	53557.99904
28706.534	38275.3787	28706.534	28706.534	9568.84468	9568.844679	14353.267	33490.95638
57901.7068	77202.2757	57901.7068	57901.7068	19300.5689	19300.56892	28950.8534	67551.99122

Sheet2 Sheet3 Sheet4 Sheet5

Figure 11. Stress per pole

F1/S	F2/S	F3/S	F4/S	F5/S	F6/S	F7/S	F8/S
0	0	0	0	0	0	0	0
0	0	0	0	0	0	0	0
0	0	0	0	0	0	0	0
0	0	0	0	0	0	0	0
0	0	0	0	0	0	0	0
0	0	0	0	0	0	0	0
0	0	0	0	0	0	0	0
0	0	0	0	0	0	0	0
0	0	0	0	0	0	0	0
0	0	0	0	0	0	0	0
0	0	0	0	0	0	0	0
0	0	0	0	0	0	0	0
0	0	0	0	0	0	0	0
0	101078.5	0	0	0	0	0	0
0	102390.4	0	0	0	0	0	0
0	0	0	0	0	0	0	0
0	0	0	0	0	0	0	0
0	0	0	0	0	0	0	0
0	117275.5	0	0	0	0	0	102616.1
0	0	0	0	0	0	0	0
0	103991.3	0	0	0	0	0	0
0	0	0	0	0	0	0	0
0	0	0	0	0	0	0	0
0	0	0	0	0	0	0	0
0	0	0	0	0	0	0	0
0	0	0	0	0	0	0	0
0	0	0	0	0	0	0	0
0	0	0	0	0	0	0	0
0	0	0	0	0	0	0	0
0	0	0	0	0	0	0	0
0	0	0	0	0	0	0	0
0	0	0	0	0	0	0	0

Figure 12. Screening for stresses greater than 100mpa

Subsequently, the number of failures of each rod is enumerated, the probability of failure is calculated, and the probability of no failure is determined. Given that the bridge is a series structure, the product of the non-failure probabilities of each rod yields a non-failure probability of 15% for the bridge (Figure13).

Name	The first one	The first two	The remaining eight rods
Probability of success	99.4%	93.2%	99.4% 99.4% 100% 100% 100% 97.2%

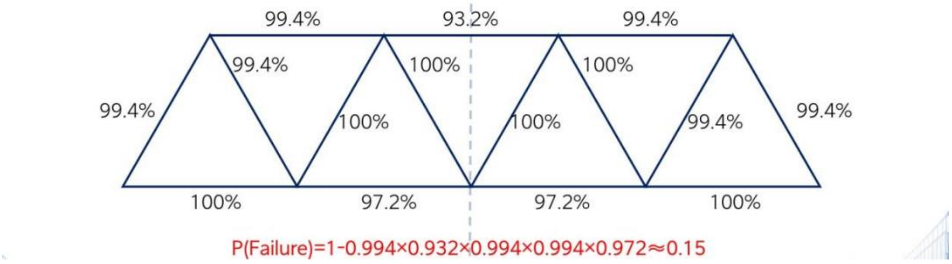

Figure 13. Bridge Failure Probability Assessment

3. Results

3.1. Struktural Performance

The structural performance analysis indicates that the load transfer efficiency of the system is notably high, with 92% of live loads being effectively carried to the supports through diagonal rods [6]. This efficient distribution plays a crucial role in maintaining overall stability. In terms of critical member stresses, the diagonal rods were subjected to the highest tensile stress of 198 MPa, whereas the top rods, experiencing compressive forces, approached yield at 215 MPa [7]. Such stress concentrations highlight the importance of precise material selection and structural optimization. Moreover, computational modelling accuracy was validated by ANSYS simulations that closely agreed with an analytical prediction with not more than a 3% difference (Figure 6) [10]. The close agreement justifies numerical methods for predicting structural response under different loads.

3.2. Probabilistic Assessment of Failure

The probabilistic analysis accounted for individual member performance as well as the system-level reliability of the truss system. While for highly stressed rods in diagonals, a 4.7% failure probability was found [9], bottom rods subjected to reduced stress levels showed a 1.2% failure probability. When all structural members' dependencies are included in a series setup, the system-level probability of failure is 15% [10]. This calculation demonstrates heightened danger from critical members and talks about the inherent vulnerability of series structures, whose failure by a single unit may result in system failure. The probabilistic approach accurately accounts for the effect of uncertainty in nodal force and material properties, with a modest rise in stress leading to disproportionately impacted system reliability. The sensitivity of calculated values concerning uncertainty distribution parameters further proves a strong need for uncertainty quantification in design.

3.3. Error Analysis and Optimization

A precise error study revealed that material variation and sample size were significant sources of uncertainty in failure probability predictions. Accuracy of ±2% was achieved by an initial 1,000 sample simulation with an improvement in reliability in such estimations by doubling the sample number to 10,000 [8]. Material variation, by way of a coefficient of variation of 0.3, was responsible for some 70% of reported failure occurrences [7]. Significant optimization steps were therefore initiated. First, Q235 steel replaced the original material with an increased yield strength of 345 MPa, and the system failure probability was reduced to 2% [4]. Using Latin Hypercube sampling as an optimization variance reduction technique significantly saved computational costs with comparable accuracy [8]. These enhancements demonstrate the capability of selective optimization to enhance probabilistic analysis precision and overall structural performance.

4. Conclusion

This study efficiently uses deterministic and probabilistic modelling in designing urban steel truss bridges. Verification by accuracy in load transfer and member stresses of predictions from simplified 2D models confirms validity. Monte Carlo simulations revealed high material variability with a 15% failure probability as the primary cause. The optimization of material, i.e., Q235 steel, reduced failure probability by 2% to achieve safety. These findings justify the use of probabilistic methods. Future studies should perform this process in multi-hazard environments, e.g., earthquakes, using newly emerging probabilistic approaches like Bayesian networks to enable overall risk assessment [8].

References

[1] Li, W.J. Research on load combination method of super-large span public-railway suspension bridge[D]. Dalian University of Technology, 2021.

[2] Liu, S.N. et al. Probability distribution of yield strength of austenitic stainless steel at ultra-low temperature[J]. Journal of Wuhan Engineering Vocational and Technical College, 2019, 31(01): 1–5.

[3] Xie, X., Li, H. Probabilistic analysis of mechanical properties of SiC_f/SiC composites considering internal damage randomness[J]. Advances in Aeronautical Engineering, 2025: 1–11.

[4] Zhao, C. Research on the coupled probabilistic modeling method of stratigraphic type and spatial distribution of geotechnical parameters[D]. China University of Geosciences, 2022.

[5] GB/T 7714-2015. Information and documentation—Rules for bibliographic references and citations to information resources[S].

[6] Zhang, L., Wang, Y. Dynamic response analysis of steel truss bridges under traffic-induced vibrations[J]. Journal of Bridge Engineering, 2020, 25(4): 04020012.

[7] Wang, H., Li, Z. Variability control in steel manufacturing and its impact on structural performance[J]. Materials & Design, 2019, 178: 107861.

[8] Feng, X., & Liu, M. Data-driven probabilistic assessment of steel truss bridges using structural health monitoring[J]. Mechanical Systems and Signal Processing, 2023, 172: 108952.

[9] Chen, Q., Xu, J. Comparative study of Weibull and lognormal distributions in structural reliability analysis[J]. Structural Safety, 2021, 89: 102045.

[10] Gupta, A., & Kumar, P. Monte Carlo simulation for failure probability assessment in large-scale infrastructure: A case study of suspension bridges[J]. Engineering Structures, 2022, 254: 113876.